Flicker source detection including fixed speed wind turbines using empirical mode decomposition

S.Z.T. Motlagh and A. Akbari Foroud*

Department of Electrical and Computer Engineering, Semnan University, Semnan, Postcode: 35131-19111, Iran.

Abstract. This study proposes an approach to identifying multiple flicker sources at the Point of Common Coupling (PCC). The voltage signals of different flicker sources such as the electric arc furnace, the fixed-speed wind turbine, and the diesel-engine driven generator were recorded at the PCC. For this purpose, various aerodynamic and mechanical faults of a wind turbine such as wind shear and tower shadow, gearbox tooth-breaking, blade crash, pitch angle error and various mechanical faults of diesel-engine driven generator such as misfiring, exciter, and governor error are considered. After acquiring voltage signals of various faults, the Empirical Mode Decomposition (EMD) as a robust signal processing technique for extracting useful features was used. Then, to reduce required memory space and computational burden, the Minimal-Redundancy-Maximal-Relevance (MRMR) and the Symmetric Uncertainty (SU) as the feature selection methods were applied. Also, to increase the efficiency of feature selection methods, the cooperative game-theoretic method was utilized. Afterward, two classifiers based on the Naïve-Bayes and the Support Vector Machine (SVM) were employed to detect the faults. Simulation results are presented to validate the effectiveness of the proposed method.

1. Introduction

1.1. Research motivation
Power quality problems such as harmonic and flicker are important issues in today's electricity systems. One of the concerns of power companies is to maintain the quality of power in the allowable range [1,2]. Flicker is a symptom of voltage fluctuation that can be produced by disturbances introduced during power generation, transmission, or distribution. However, it

is generally caused by the use of fluctuation loads, i.e., loads that work periodically, like wind turbines and arc furnaces [3]. Also, flicker phenomenon can appear in electrochemical systems as an inherent property [4]. According to the IEEE standard 100-1977 and IEC 610004-15, the voltage flicker is defined as the impression of fluctuating brightness or color that occurs when the frequency of observed variation lies between a few hertz and the fusion frequency of images [5].

1.2. Literature review
Many techniques for the detection of flicker sources have been presented. In [6], Auto-Regressive Moving Average (ARMA) model was applied for modeling the variations of active and reactive powers and also, a new index based on the power spectral densities was

---

*. Corresponding author.
  E-mail addresses: sztmotlagh@semnan.ac.ir (S.Z.T.
  Motlagh); aakbari@semnan.ac.ir (A. Akbari Foroud)

used for identifying flicker sources. This method needs to record multiple voltages of different buses so that computational burden and memory storage can be increased. In [7], an approximate equivalent circuit of the line between the monitoring points via Wavelet Transform (WT) was calculated and then, flicker sources were detected based on the data of voltage and current of the system. However, this approach is time-consuming and suffers from a high computational burden due to the use of both voltage and current of more than one monitoring point. In [8], a discrete version of the Continuous Wavelet Transform (CWT) was used to calculate the low-frequency oscillations of flicker components of voltage and current signals; after that, flicker power was used to find the location of flicker sources. However, this method is subject to a heavy computational burden. In [9], voltage and current signals were computed and then, the Fast Fourier Transform (FFT) was applied to compute the complex power of a specified bus. Therefore, with the acquired information, a flicker source was identified. However, not only this method is time-consuming but also only one flicker source can be detected. In [10], the WT and flicker power were used to detect flicker sources. However, different types of flicker sources were ignored. In [11], the S-Transform (ST) was employed to detect the flicker components and artificial neural networks were applied to classify the bus with the flicker source. This method needs different measurement points. The ST suffers from computational complexity, and a relatively fixed Gaussian window causes a lack of time-frequency resolution for different non-stationary signals [12,13]. Besides, only one source of flicker was considered for the detection. In [14], flicker power was measured, which could help identify the flicker source. However, in this method, more than one measurement equipment was used; thus, the speed of the process was reduced and the memory requirement increased. In [15], non-parametric statistical analyses of voltage changes and kernel density estimation were used for identification. This method needs more than three measurement points to acquire enough information for locating flicker sources. It should be noted that the methods mentioned above need more than one measurement point to collect enough data for detecting flicker sources. Besides, they used signal analyzers (such as ST, WT, CWT) that coud not provide sufficient information on the issue of time. In [16], the authors studied the impact of wind shear and tower shadow on output power in various wind turbine faults. Furthermore, the flicker produced by some mechanical factors such as blade break down, blade pitching, and gearbox tooth crash were studied. However, the identification of multiple flicker sources was ignored while only six classes were investigated. Besides, they used the ST and the WT

to extract features, leading to more processing time and memory space. The authors in [17] studied factors that could produce flicker in Diesel-Engine Driven Generators (DEDGs). These factors were inherent torque fluctuations and mechanical factors (misfiring, exciter, and governor error). Besides, they presented a method by analyzing voltage waveforms based on the Discrete Wavelet Transform (DWT) and Discrete S-Transform (DST) for the detection of the faults mentioned above. The mmentioned paper restricted its approach to using two signal processing techniques for extracting useful features and utilizing Gram Schmidt feature selection, which is a wrapper method causing more computational burden [18]. The aforementioned papers suffer from the straightforward procedure that needs low-processing time and low computational burden. Also, the multiple flicker sources that contain different flicker sources, such as wind turbines, have been neglected.

Consequently, this paper aims to propose an effective, straightforward and fast method based on the only voltage waveforms of the Point of Common Coupling (PCC) for detecting multiple flicker sources that contain fixed-speed wind turbines. Also, the proposed method does not suffer from the issues that are mentioned above. According to the referenced findings [16], for acquiring beneficial features that can help identify wind turbine flicker sources, the ST or the WT cannot provide adequate information alone, and both should be applied together to acquire enough data. The Empirical Mode Decomposition (EMD) is a time-frequency analysis method that breaks down signals into components called Intrinsic Mode Functions (IMFs). In this technique, the sifting process is used for converting stationary, non-stationary, and linear and nonlinear signals into mono components. This method is subject to a number of advantages such as being adaptive, direct, simple and intuitive. Therefore, according to the drawbacks of the other signal processing techniques that are mentioned above and the advantages of the EMD, the EMD algorithm has been chosen.

1.3. Novelty and main contribution

In this paper, a method to recognize different sources of flicker at the PCC is presented, which only uses voltage waveform. The proposed method can identify flicker sources that are produced by wind turbine aerodynamic factors (wind shear and tower shadow), wind turbine mechanical faults (blade crash, tooth crash of gearbox, and the error of pitch control), the DEDG mechanical faults (misfiring, governor, and exciter errors), and also voltage flicker produced by the Electrical Arc Furnace (EAF) [19–21]. Moreover, the purpose of this article is to introduce an algorithm that can detect the faults mentioned above and different

flicker sources can be added to the scheme for the identification of flicker sources. All of the mentioned faults are simulated by changing some parameters like blade crash length, the number of broken teeth, pitch angle fluctuations frequency, misfired cylinders' number, misfiring severity, and the amount of fuel to cover probable states. Then, voltage signals are acquired from direct metering at the PCC. These signals can be used for fault detection because they are obtained from different faults that have distinct attributes. In order to identify the fault types, an appropriate pattern recognition method is presented. In this method, the beneficial features from fault signals are extracted using the EMD [22]. One of the essential steps in pattern recognition and machine learning is feature selection, also known as variable selection. Some of the features in the dataset are redundant and irrelevant, hence more computational burden and low efficiency. Thus, a proper feature selection method is used to select effective features. In this study, the MRMT and the SU, which are optimized by the cooperative game-theoretic method [23], are employed for selecting the most important features. Afterward, the Naïve Bayes and the Support Vector Machine (SVM) are employed as representative classifiers for the detection of faults. Finally, the type of fault as the flicker source could be identified by the output of the classifiers. Of note, every flicker sources have distinctive signals that can be decomposed into different modes through the EMD (signal processing technique). Then, from each mode, different features can be extracted. Therefore, every source has its own unique features that are not equal to other flicker sources. These distinctive features are used for training the classifier. Consequently, another flicker source can be added without affecting the performance of the classification accuracy. The main steps of flicker source detection are shown in Figures 1 and 2. The main contributions of this paper are as follows:

- Presenting a method to recognize the different sources of flicker in the presence of the fixed speed wind turbines at the PCC. The proposed method not only can identify the important factors that produce flicker (different faults of wind turbines and DEDG, and flicker produced by the EAF), but also other flicker sources can be added simply to the scheme for the identification of flicker sources;

- The proposed method is categorized in a single-point method category. In the proposed method, only voltage waveforms at the PCC are used. As a result, it can help reduce the memory requirement and increase computational speed;

- The proposed technique uses the EMD for feature extraction due to its simplicity and also, its

mathematical basis is not complex. Hence, the computational complexity is reduced;

- Feature selection can help eliminate the redundant data; hence, the classification accuracy and the computational speed increase and the required memory is significantly reduced;

- The obtained results indicate high classification accuracy.

1.4. Organization of the paper
The remainder of this context is organized as follows: Section 2 presents the details of the test circuit. In Section 3, the major faults that lead to flicker in a power system are modeled. In Section 4, the EMD method and the feature extraction approach are explained. In Section 5, feature selection methods are described in detail. In Section 6, the classification methods that have been used in this paper are presented. In Section 7, classification results and the performance evaluations of the proposed method are presented. In Section 8, the proposed method is compared those in other papers and finally, the paper is concluded in Section 9.

2. Test system

In this paper, a wind turbine and a DEDG are connected to a weak network via 2.5-km lines. Also, an EAF is directly connected via a 15 MVA, 0.58/20 kV grounded-wye-grounded-wye transformer with leakage inductance of 5% and also a 3 MVA load with a power factor of 0.97 is connected at the PCC. Table 1 presents the numerical data set on the simulated system. The network has been deliberately chosen to be weak to investigate the effect of the mentioned factors on the flicker event [24,25]. This study employed a capacitor voltage transformer (CVT) for metering voltage signals. The utilized CVT is available in PSCAD/EMTDC. In this CVT, Eddy Loss, Air-Core Reactance, Knee Point Voltage, and Burden are considered. The network short-circuit power is selected to be 15 MVA, and also X/R ratio is equal to 7.5. Figure 3 shows the simulated test network details in PSCAD/EMTDC software, and Figure 4 depicts a single-line diagram of the system.

Table 1. Specifications of the simulated system.

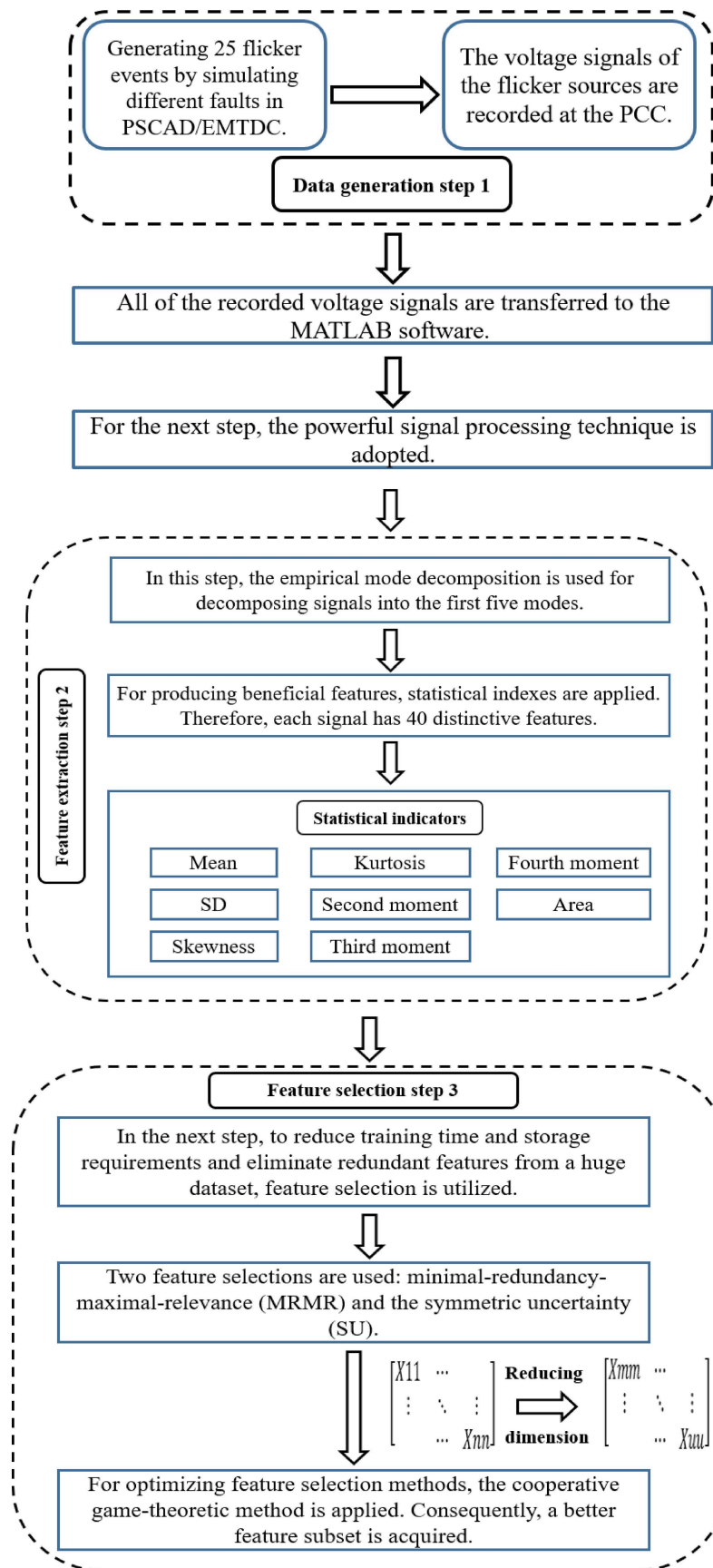| Parameters	Characteristics
Line 1-2 impedance	0.313 + 0.260j
Line 1-3 impedance	0.313 + 0.260j
Load capacity	3 MVA
System frequency	60 Hz
Network short circuit power	15 MVA
Grid voltage	69 kV

Figure 1. Structure of the proposed algorithm for flicker source classification.
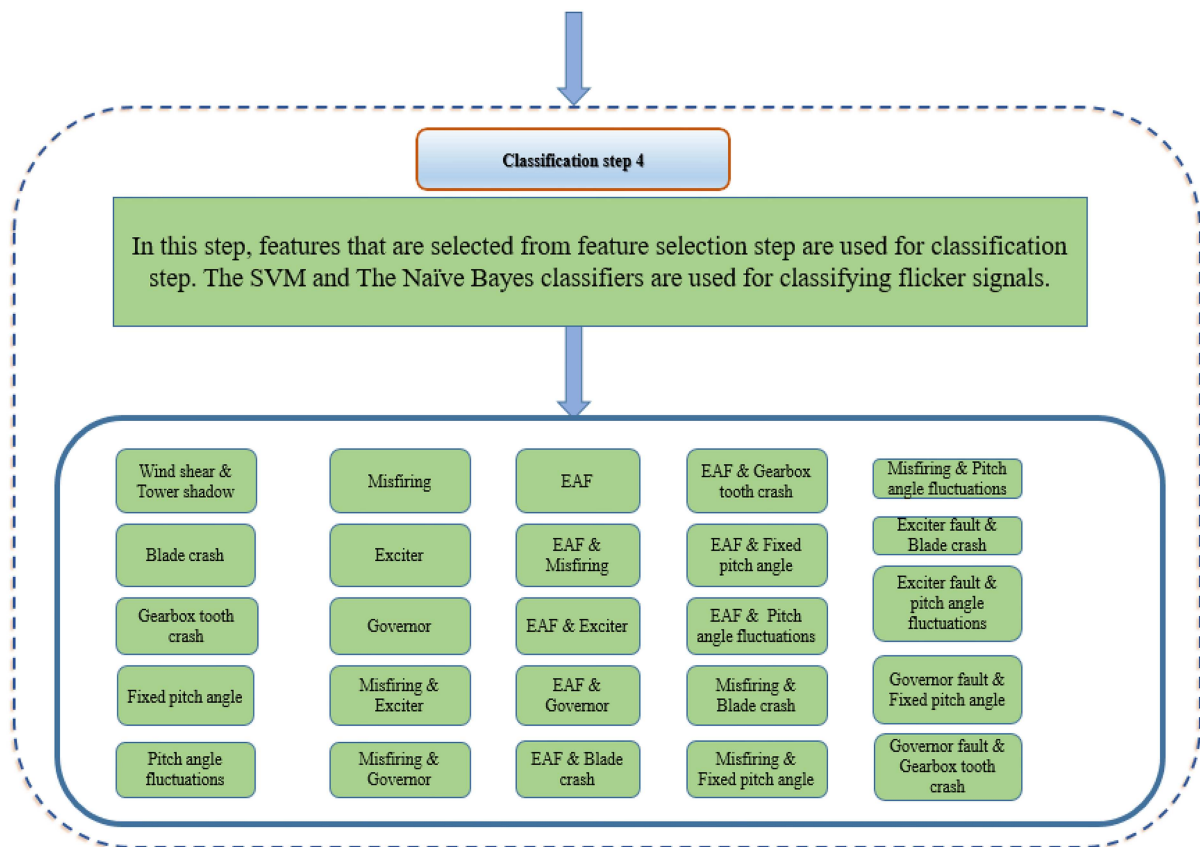
Figure 2. Continuation of the previous figure.

3. Modeling and simulating the faults

This section is divided into three subsections. In Section 3.1, wind turbine faults that include wind shear and tower shadow, blade crash, gearbox tooth crashing, and pitch control errors are simulated. It is notable that all of the faults of the wind turbine are modeled in the presence of the wind shear and tower shadow, which occur at the same time. In Section 3.2, the DEDG faults that include misfiring error, exciter fault, and governor error are simulated. In Section 3.3, an EAF model that can be modeled in the PSCAD software environment is presented.

3.1. Wind turbine faults

Wind turbines significantly influence power quality. There are some factors that cause voltage flicker. These factors can be classified into three main categories: the turbine's aerodynamic, mechanical, and electrical factors. In this paper, a squirrel cage induction generator is driven by a wind turbine. Type 1 out of 4 types of wind turbines (the fixed speed wind turbine) is simulated in the PSCAD/EMTDC based on IEC 61400-27, which is standard for electrical simulation models of wind turbines [26–33]. Table 2 shows the parameters for the wind turbine model. Wind shear and tower shadow are aerodynamic factors. Mechanical

Table 2. Parameters of the wind turbine model.

Parameters	Value
Blade radius	38 M
Tower radius	2 M
Hub height	70 M
Wind shear component	0.3
Blade origin from tower midline	3 M
Gear ratio	75
Generator-rated power	2 MW
Generator-rated voltage	0.398 KV
Generator pole pairs	3
Nominal frequency	60 Hz

factors include the error of the blade pitching, blade crashing, and failure of the gearbox. The third factor constitutes switching devices such as inverters. The model of wind speed has been fallen into three components: hub height wind speed, wind shear, and tower shadow.

3.1.1. The model of the hub height wind speed

The wind turbine hub height is the rotor's height above the ground. Commonly, the wind speed increases with
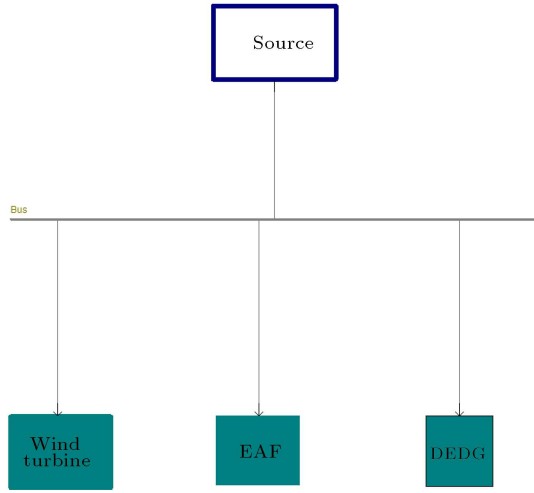
Figure 3. The PSCAD/EMTDC simulation model of the test system.

height. For this reason, there is a strong motivation for increasing turbine hub heights to capture extra energy from the wind. Eq. (1) presents the wind speed in hub height [34]:

$$v_{eq_0} = \frac{2V_h}{3R^2} \sum_{b=1}^{3} \int_0^R r\,dr = V_h. \qquad (1)$$

3.1.2. Wind shear
Wind speed typically augments with height and this

variation is known as wind shear. The blades of the wind turbine encounter maximum wind speed when facing upward, while if facing downward, they encounter minimum wind speed. If none of the blades breaks, the impact of the wind shear on output power is insignificant [35]. A common wind shear model is expressed in Eq. (2):

$$\frac{v}{v_{ref}} = \left(\frac{H}{H_{ref}}\right)^a, \qquad (2)$$

Figure 4. Single-line diagram of the system.

where v is wind speed at elevation H, v_{ref} wind speed at an elevation H_{ref}, and a the friction factor. Eq. (3) shows the final wind shear equation based on the mean wind speed.

$$v_{eq_{wshear}} = V_h \left[\frac{a(a-1)}{8} \left(\frac{R}{H} \right)^2 \right.$$

$$\left. + \frac{a(a-1)(a-2)}{60} \left(\frac{R}{H} \right)^3 \cos 3\theta_b \right]. \qquad (3)$$

3.1.3. Tower shadow
The airflow experienced by a turbine blade is modified due to the presence of the tower. This effect is called tower shadow. For a three-blade turbine, this reason is the cause of the output power fluctuations. On an upwind turbine, when the blade is directly in front of the tower, torque pulsations are not very severe. For the downwind rotor, the tower shadow is more obvious. The model of this event was developed in [34] and expressed in Eq. (4):

$$v_{eq_{tshadow}} = \frac{V_h}{3R^2} \sum_{b=1}^{3} \left[\frac{a^2}{\sin^2\theta_b} \ln \left(\frac{R^2 \sin^2\theta_b}{x^2} + 1 \right) \right.$$

$$\left. - \frac{2R^2 a^2}{R^2 \sin^2\theta_b + x^2} \right]. \qquad (4)$$

Wind shear and tower shadow take place at the same time and both of them influence Power Quality Disturbances (PQDs), especially flicker [36]. The complete wind model is the sum of the three mentioned components and is shown as Eq. (5):

$$v_{eq} = v_{eq_0} + v_{eq_{wshear}} + v_{eq_{tshadow}}$$

$$= V_h + V_h \frac{a(a-1)}{8} \left(\frac{R}{H} \right)^2 \frac{a(a-1)(a-2)}{60} \left(\frac{R}{H} \right)^3$$

$$\cos 3\theta_b + \frac{V_h}{3R^2} \sum_{b=1}^{3} \left[\frac{a^2}{\sin^2\theta_b} \ln \left(\frac{R^2 \sin^2\theta_b}{x^2} + 1 \right) \right.$$

$$\left. - \frac{2R^2 a^2}{R^2 \sin^2\theta_b + x^2} \right]. \qquad (5)$$

3.1.4. Blade crash
To improve power quality and reduce maintenance costs, all blades must be in good condition. If blades do not have a healthy structure due to breakdown, the output power from the wind turbines experiences oscillation. Moreover, if the length of the crashed blade exceeds a limit, the tower will collapse. For this reason, in this paper, the length of the broken piece is considered a maximum of 6 m. Hence, Eq. (5) is modified and the final equivalent wind speed model will be expressed in Eq. (6) [16]. In this equation, the R for two of the blades is considered 38 m and R_b is assumed to be the broken blade, which varies from 32 m to 37 m.

$$v_{eq} = v_{eq_0} + v_{eq_{wshear}} + v_{eq_{tshadow}} = \sum_{b=1}^{3} \left[\frac{V_h R_b^2}{3R^2} \right]$$

$$+ \left[\left(\frac{2V_h}{3R^2} \right) \frac{aR_b^3}{3H} \cos\theta_b + \frac{a(a-1)R_b^4}{8H^2} \cos^2\theta_b \right.$$

$$\left. + \frac{a(a-1)(a-2)R_b^5}{30H^3} \cos^3\theta_b \right]$$

$$+ \left[\left(\frac{2V_h}{3R^2} \right) \left(\left(1 + \frac{a(a-1)R^2}{8H^2} \right) \right. \right.$$

$$\left(\frac{a^2}{\sin^2\theta_b} \ln \left(\frac{R^2 \sin^2\theta_b}{x^2} + 1 \right) \right.$$

$$\left. \left. \left. - \frac{2R^2 a^2}{R^2 \sin^2\theta_b + x^2} \right) \right) \right]. \qquad (6)$$

3.1.5. Gearbox tooth-breaking
A gearbox is used to convert a slow-speed, high-torque wind turbine rotation into a turbine that enjoys higher speed and lower torque required by most generators to produce electricity. Gearbox tooth crashing in the wind turbine causes fluctuations in the output power because the torque cannot be transmitted from the shaft of the turbine side to the drive shaft of the generator side at a specific time. Since one of the M gears is crashed, the transferred torque can be expressed as follows [37]:

$$T = \begin{cases} T_0, & 0 \le t \le \frac{M-1}{M}\tau \\ 0, & \frac{M-1}{M}\tau \le t \le \tau \end{cases} \qquad (7)$$

where $\tau = 2\frac{\pi}{\omega}$ and ω is the speed of the shaft.

3.1.6. Pitch control
Pitch control is a mechanism used to operate and

adjust the angle of blades in a wind turbine, which helps regulate the output power and protect the rotor blades. The turbine's electronic controller monitors the output power multiple times per second. If the output power becomes too high, the controller sends a signal to slightly adjust the rotor blades out of the wind. Similarly, if the wind speed decreases, the blades will turn back toward the wind. The power as a function of the wind is described by Eq. (8) [38]:

$$p = 0.5\rho\pi V_{wind}^{\ 3}C_p, \tag{8}$$

where ρ is the air density, R the wind turbine rotor radius, and V_{wind} the wind speed. However, part of the power from the wind can be extracted from the wind turbine. Thus, the extracted power is expressed as follows:

$$P = 0.5\rho\pi R^3 V_{wind}^{\ 3}C_p\left(\beta, \gamma\right), \tag{9}$$

where C_p is the aerodynamic efficiency of the rotor (power coefficient), β the pitch angle of the rotor blades, and γ the tip speed ratio. The value of $C_p\left(\beta, \gamma\right)$ is calculated as [39]:

$$C_p = \frac{1}{2}\left(\gamma - 0.022\beta^2 - 5.6\right)e^{-0.17\gamma}, \tag{10}$$

where:

$$\gamma = 2.237 \times \frac{V_{wind}}{hub\,speed}. \tag{11}$$

Eqs. (9) and (10) illustrate the relation between the pitch angle and the output power, and pitch control error can cause power quality issues.

3.1.7. Pitch angle fluctuations and fixed pitch
As mentioned above, these faults can cause voltage fluctuations due to the interconnection among the voltage, the output power, and the pitch angle. To simulate the pitch angle at the fixed angle in the PSCAD/EMTDC, the governor of the wind turbine is deactivated and the value of the angles changes from 0–20°. Likewise, the frequency of the pitch angle is changed between 2–10 rad/s to simulate pitch angle fluctuations.

3.2. DEDGs faults
In this article, misfiring, governor, and exciter error of the DEDG that cause flicker events are modeled. In the case of the diesel engine, a 3 MWA, 12-cylinder and four-stroke diesel engine is simulated. According to Figure 3, two switches are considered for activating the constant active or reactive power mode synchronous generator. In the constant reactive mode, if switch one is activated, the exciter will be disconnected and the fixed voltage source will feed the exciting winding. Also, for the constant active mode, when switch two is on, the connection between the diesel engine tank and the governor output is disconnected; then, the fixed

Table 3. Parameters of the DEDG model.

Parameters	Characteristics
Engine type	four stroke-12 cylinders
Engine rated power	3 MW
Engine rated speed	900 rpm
Gearbox efficiency	0.97
Gearbox ratio	10
Exciter model	Static exciter1A
Generator rated power	3 MVA
Rated voltage	13.86 kV
Governor model	DEH controls
System frequency	60 Hz

fuel feeds the engine tank. Thus, the speed of the generator shaft remains constant. Table 3 presents the specification of the DEDG.

3.2.1. Misfiring
Misfiring is a phenomenon engendered by a lack of combustion in the cylinder owing to the lack of spark energy, low compression pressure, imbalance in the air-to-fuel ratio, or mechanical issues such as problems in cylinder walls. According to referenced studies [40,41], misfiring causes torque fluctuations and the frequency of fluctuations rises upon adding more misfired cylinders. Moreover, misfiring causes voltage variations, which lead to voltage flicker. In the simulation tool of the PSCAD/EMTDC, the number of misfiring cylinders can be adjusted along with the given mechanical torque individually.

3.2.2. Governor mechanical fault
In an electric power system, synchronous generators convert mechanical energy into electrical energy. Reference speed is compared with the speed of the synchronous generator by a governor, which regulates fuel input to the engine. The constant active mode should be activated to simulate governor error by disabling the governor and feeding the engine with a fixed amount of fuel. In addition to this fault, a misfiring fault occurs and increases the magnitude of variations. Therefore, to dampen the fluctuations, the system needs the governor.

3.2.3. Exciter mechanical fault
The excitation system is defined as the system that is used for the satisfaction of the power system by controlling the field voltage, which results in controlling the field current. Therefore, reference voltage and voltage of generator windings are compared together by exciter, after which the voltage of exciting windings can be adjusted. This fault is a constant reactive power mode, and to simulate exciter error, the exciter

should be disabled, which causes the magnitude of fluctuations to increase and the fixed voltage feeds the windings of the generator exciting system. Also, the misfiring can happen with an exciter fault. In this case, the exciter cannot react to the misfiring fault; therefore, the severity of fluctuations will be increased significantly [17].

3.3. EAF

The EAF is a highly variable nonlinear load that causes power quality issues, especially voltage flicker. Analysis of the EAF loads illustrates rapid reactive power variations and also, the reactive power drawn by the furnace can influence the feeding voltage and, therefore, cause a voltage drop on the primary side of the transformer of the EAF, leading to fluctuating terminal voltages. In this article, an accurate model of the EAF is modeled, which can be incorporated in the PSCAD software. The equations for the electric arc are expressed below [42]:

$$k_1.r^n + k_2.r.\frac{d_r}{d_t} = \frac{k_3}{r^{m+2}}.i^2, \qquad (12)$$

$$v = \frac{k_3}{r^{m+2}}.i, \qquad (13)$$

where $m, n, k_1, k_2,$ and k_3 are model constants, r the arc radius in centimeters, v the voltage across the arc in Volts, and i the current through the arc in Amperes. It should be noted that the EAF generates 7 MVA arc power and the model parameters are presented in Table 4.

4. Feature extraction based on EMD

The feature extraction technique is the key to pattern recognition because it extracts distinctive information from input data. If the extracted features are not helpful, then the performance of the classifier will be unacceptable. The algorithm of the EMD is established on the hypothesis that any data comprise different intrinsic mode oscillations [43]. It converts nonlinear and non-stationary signals into their respective single components and symmetric components via the sifting process. The EMD sieves out a given signal into its constituent mono components, comprehending a

Table 4. The EAF model parameters.

Parameters	Phase A	Phase B	Phase C
m	0	0	0
n	2	2	2
K_1	2900	2900	2900
K_2	1	1	1
K_3	17.5	17.5	17.5

narrow band of frequencies. Each component is called the IMF. The IMF must satisfy the following two conditions:

a) In the whole data set, positive/negative peaks and the number of zero crossings must be either equal or differ by one at most;

b) At any point, the mean value of the envelope determined by the local maxima and the envelope determined by the local minima should be zero.

The steps to obtain the IMF can be demonstrated as follows [44]:

1. Determine local maxima and minima of the distorted signal, $u(t)$;

2. Find upper and lower envelopes by performing cubic spline interpolation between the maxima and the minima, as denoted by $e_{up}(t)$ and $e_{low}(t)$, respectively;

3. Calculate the mean of the envelopes as: $h(t) = (e_{up}(t) + e_{low}(t))/2$;

4. Extract the detail $d_i(t) = u(t) - h(t)$;

5. If $d_i(t)$ satisfies the IMF basic requirements, then the new IMF is described as: $c_i(t) = d_i(t)$;

6. Compute residue, $r_i(t) = u(t) - c_i(t)$;

7. Increase the IMF count (i) by one; after that, repeat Steps 1-6 with $r_i(t)$ as the new original signal to obtain the next IMF and a new residue.

The stopping criterion for the above procedure is when $r_i(t)$ becomes a monotonic function. This indicates that no further IMFs can be extracted from the signal. Figures 5-11 show the first 5 IMFs of 6 different faults. The first five IMFs have been chosen through trial and error. Also, the investigations illustrate that using more modes would not change classification accuracy. Also, they caused greater computational complexity and processing time. In this literature, the EMD method is applied to obtain the first five IMFs and then, various features are extracted from the IMFs. For instance, several statistical features like Standard Deviation (SD), skewness, and moments of second- to fourth-order of the IMFs are extracted. Therefore, a total of 40 features are extracted from the analyzed voltage signals. The extracted features are shown in Table 5. These features are used because many references, such as [22,45], have proved their efficiency.

5. Feature selection step

The main purpose of feature selection is to find significant features that improve the performance of classifiers. The advantages of feature selection may

Figure 5. Voltage waveforms of the EAF along with their IMF 1–5.

Figure 6. Voltage waveforms of the wind turbine: Pitch angle fluctuations 8 rad/s along with their IMF 1–5.
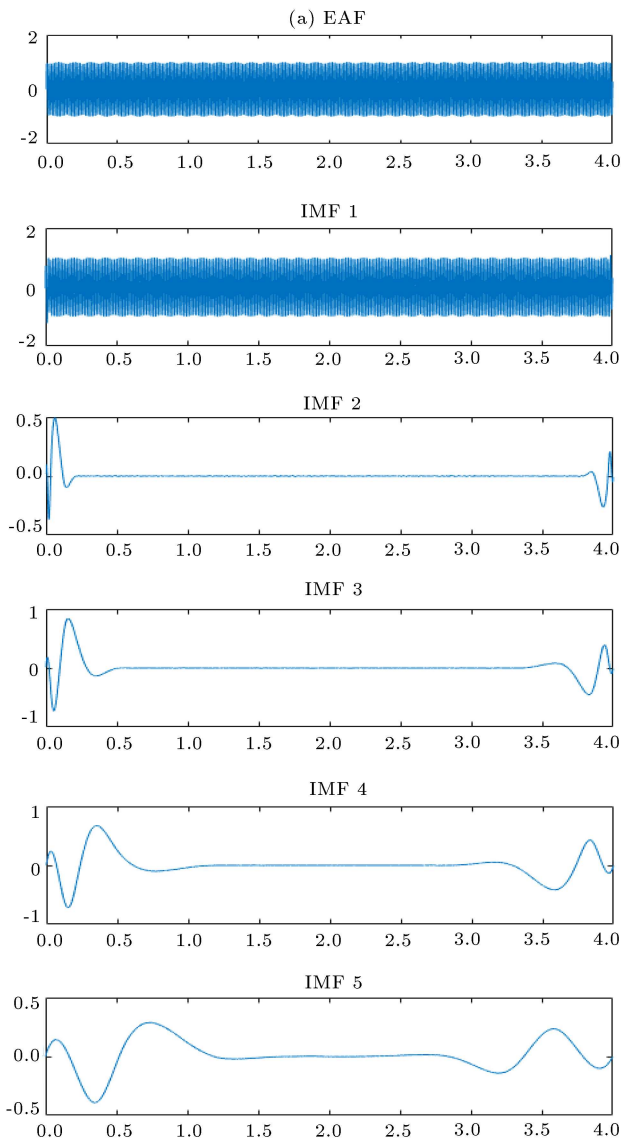
include reducing training time and storage requirements and eliminating redundant features from a huge dataset [46]. Typically, feature selection methods are categorized into three groups: embedded, wrapper, and filter methods. Embedded methods are usually specific to a single learner. Wrapper methods convolve with the classifiers and reduce the error of the classification. By using a learning algorithm to guide the search, they explore the feature subset space. Both the wrapper and the embedded methods are subject to certain drawbacks, such as high computational complexity and poor generalization ability. Filter methods select features regardless of the employed data modeling algorithm. Filter methods do not rely on learning algorithms, and also the relevance of features is evaluated by investigating the intrinsic properties of the data. Filters are less computationally intensive than wrappers, yet
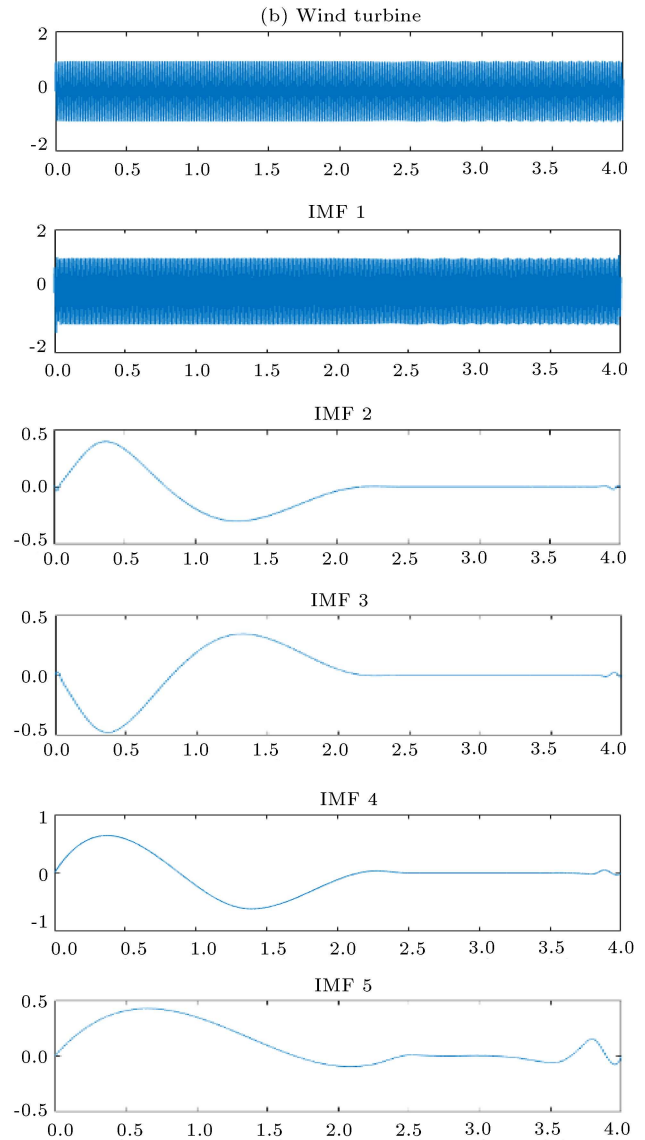
they can achieve comparable classification accuracy for most classifiers. Hence, filter methods are used widely for high-dimensional datasets. However, filter selection algorithms often neglect some features which are weak as individuals; nonetheless, they have high discriminatory power when considered as a group. To overcome this problem, Sun et al. [23] developed a framework in which the weight of each feature is evaluated using the cooperative game-theoretic method based on the Shapely value. After evaluating the weights of the features, they are sent to the feature selection algorithm. In this paper, this method is used for the feature selection step.

5.1. Cooperative game theory concepts

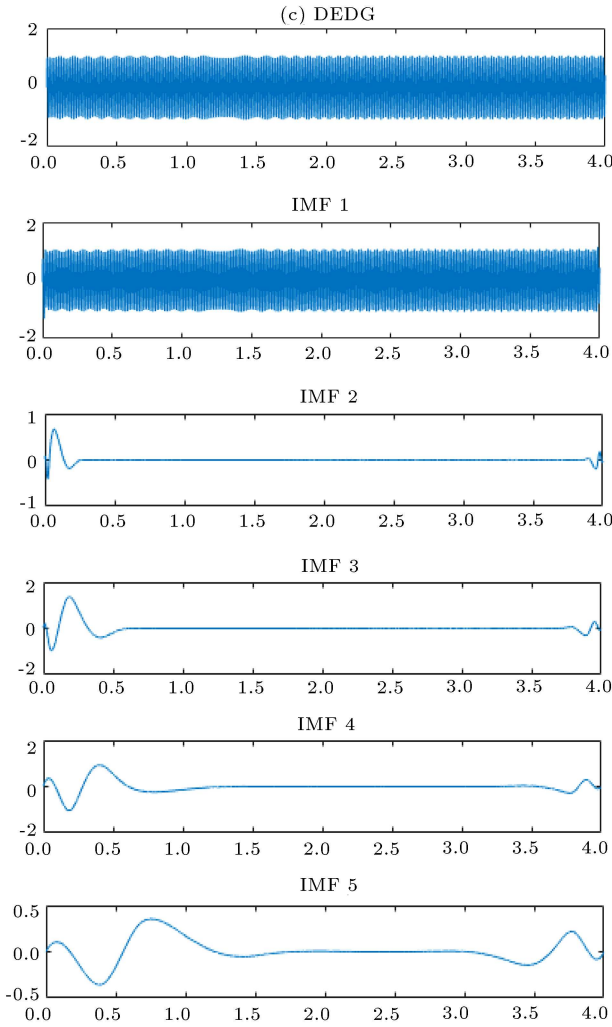Game theory is a field of mathematics that is applied to analyze conflicts between self-interested decision-

Figure 7. Voltage waveforms of the DEDG: Misfiring 1-4-7-10 along with their IMF 1-5.

Figure 8. Voltage waveforms of the EAF-Wind turbine: EAF & pitch angle fluctuations 8 rad/s along with their IMF 1-5.

makers, also known as players, who interact with each other. $N = \{1, 2, ..., N\}$ is the set of players called coalitions, which can make binding agreement about joint strategies. The game is created with a pair $N = (N, V)$ and $v : 2^N \rightarrow R$ is the characteristic function. For each subset of players $S \subseteq N, v(S)$ is the amount that the members of S can earn by working together. The value of $v(S)$ for the empty coalition is zero, which is $v(\phi) = 0$. Shapley offered an approach (The Shapley value) in the Cooperative Game Theory (CGT) to yield a unique outcome in the coalitional game [47].

5.2. Shapley value in the feature selection

The Shapley value is a method that fairly distributes both costs and rewards among players. In the case of feature selection, each subset can be the optimal subset and the importance of every feature (based on the intrinsic correlative structures among features) is estimated via Shapley value. The equation of Shapley value is expressed as follows:
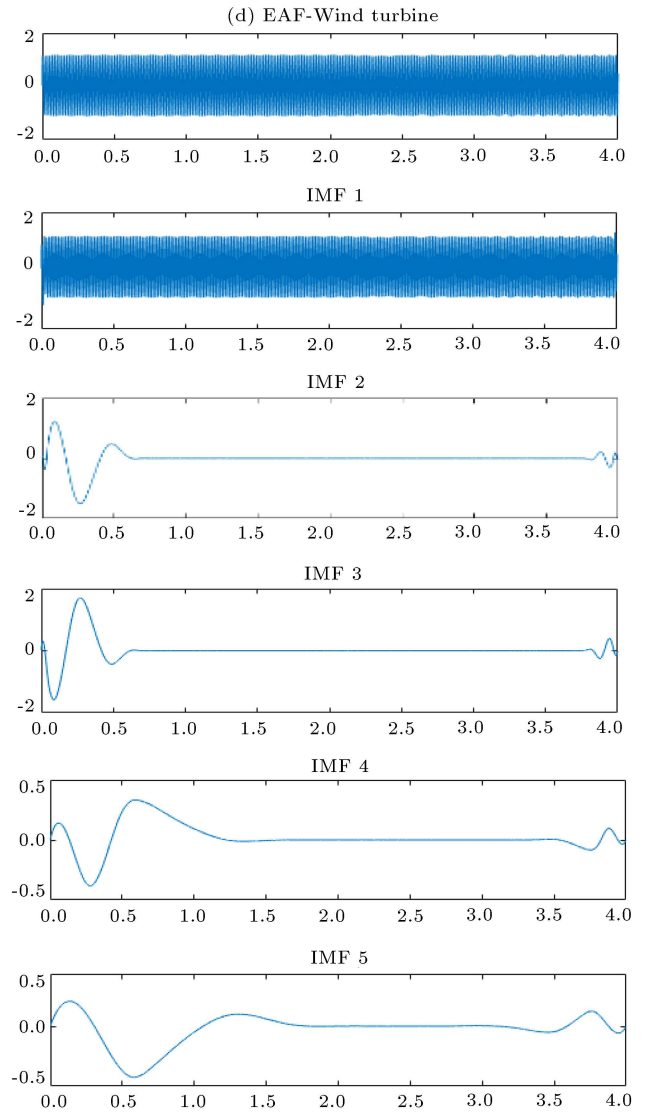
$$\phi_i(v) = \sum_{S \subset N} \left(v\left(S \cup i\right) - v\left(S\right) \right) \left(\frac{|S|!(n - |S| - 1)!}{n!} \right), \, (14)$$

where $\phi_i(v)$ is the payoff of Shapley value to the ith player and n is the whole number of the players. Also, the $(v\left(S \cup i\right) - v\left(S\right))$ is defined again in the context of feature selection and shown as [23]:

$$\psi(i, j) = \begin{cases} 1, & I\left(f_j; class \,|f_i\right) > I\left(f_j; class\right) \\ 0, & else \end{cases} \quad (15)$$

and:

$$(v\left(S \cup i\right) - v\left(S\right)) =$$

$$\begin{cases} 1, & I\left(S; class; f_i\right) \geq 0 \text{ and } \sum_{f_j \in S} \psi(i, j) \geq \frac{|S|}{2} \\ 0, & else \end{cases} \quad (16)$$

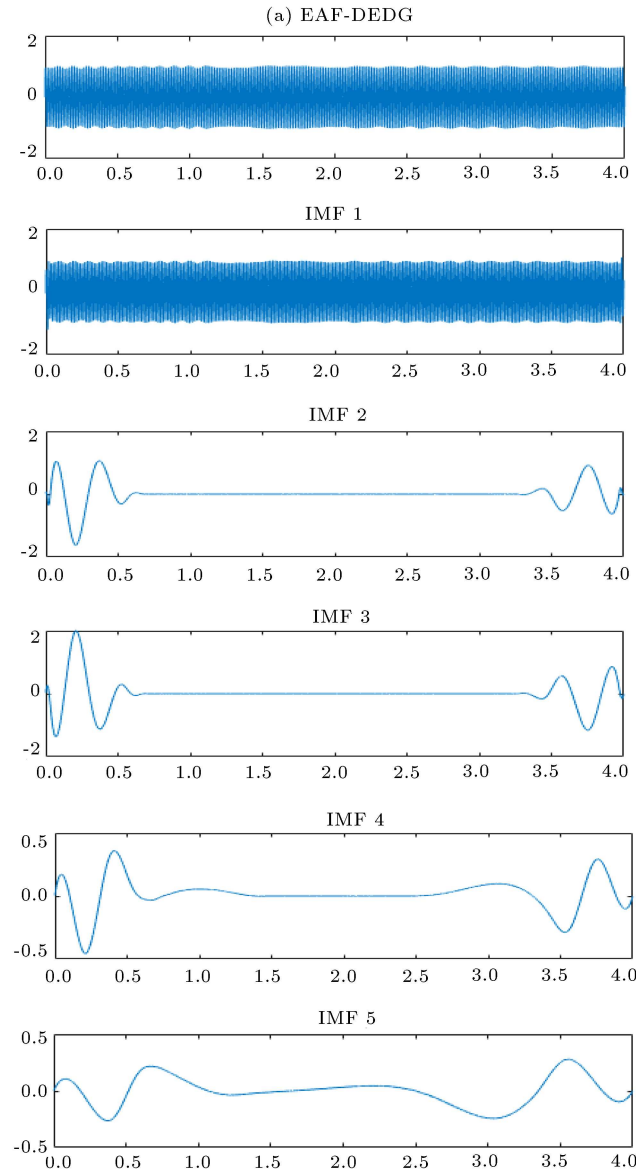where $\psi(i, j)$ is the independence index, I is the mutual

Figure 9. Voltage waveforms of the EAF-DEDG: EAF & misfiring 1-4-7-10 along with their IMF 1-5.

information, and the algorithm of a general feature selection optimization with the CGT is presented in the following [23]:

Input: A sampling dataset
Output: Subset M (the most important features)

1) Initializing: $M = \phi$ and $k = o$

2) While $k < \gamma$ do

3)   For each feature, $f_i \in G$ do

4)   Compute $Q(f_i)$;

5)   Compute $N(f_i) = Q(f_i) \times w(i)$;

6)   End
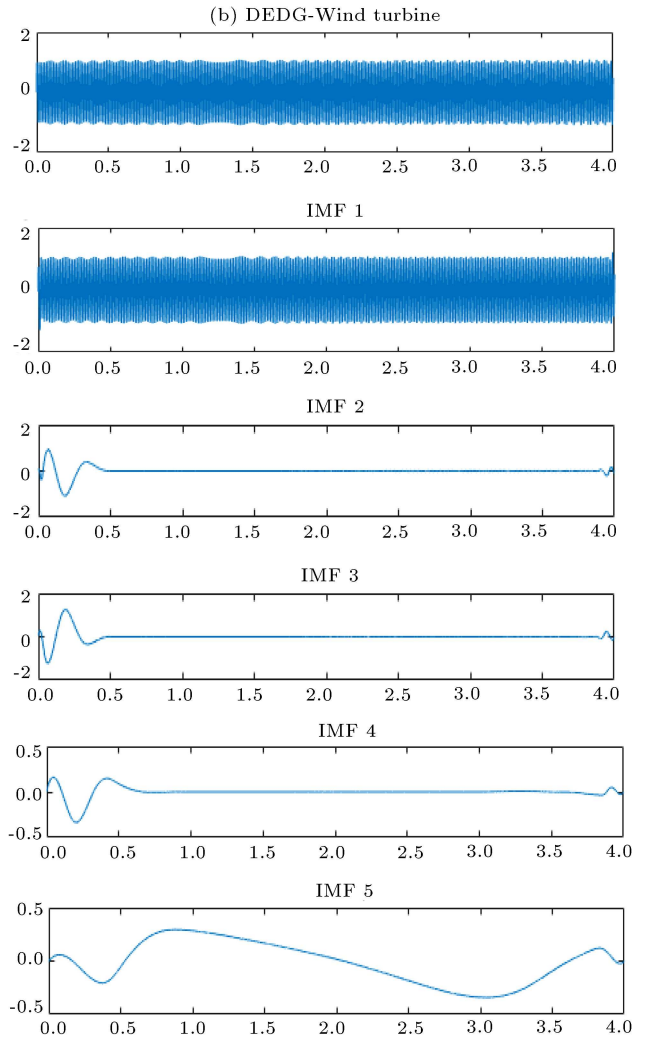
7)   Pick the feature f_i with the highest $N(f_i)$;

Figure 10. Voltage waveforms of the DEDG-Wind turbine: Misfiring 1-4-7-10 & pitch angle fluctuations 6 rad/s along with their IMF 1-5.

8) $M = M \cup \{f_i\}$;

9) $k = k + 1$;

10) End

The $p = (G, L, C)$ is assumed as the sampling dataset, where (G, L, C) are the sets of features, instances, and target classes, respectively, and also $w(i)$ is the Shapley value of the feature f_i. The parameter γ is a threshold that is used to terminate the procedure. For selecting the best feature in each iteration, the function $N(f_i)$ is determined to estimate the dominance of each feature over others. The information criterion function $Q(M)$, like the Minimal-Redundancy-Maximal-Relevance (MRMR) [48] and the Symmetric Uncertainty (SU) [49], is employed to choose feature f_i according to feature relevance and redundancy or relevance analysis. In this article, a general feature selection method with the CGT is used and the MRMR and the SU are utilized as the criterion functions to
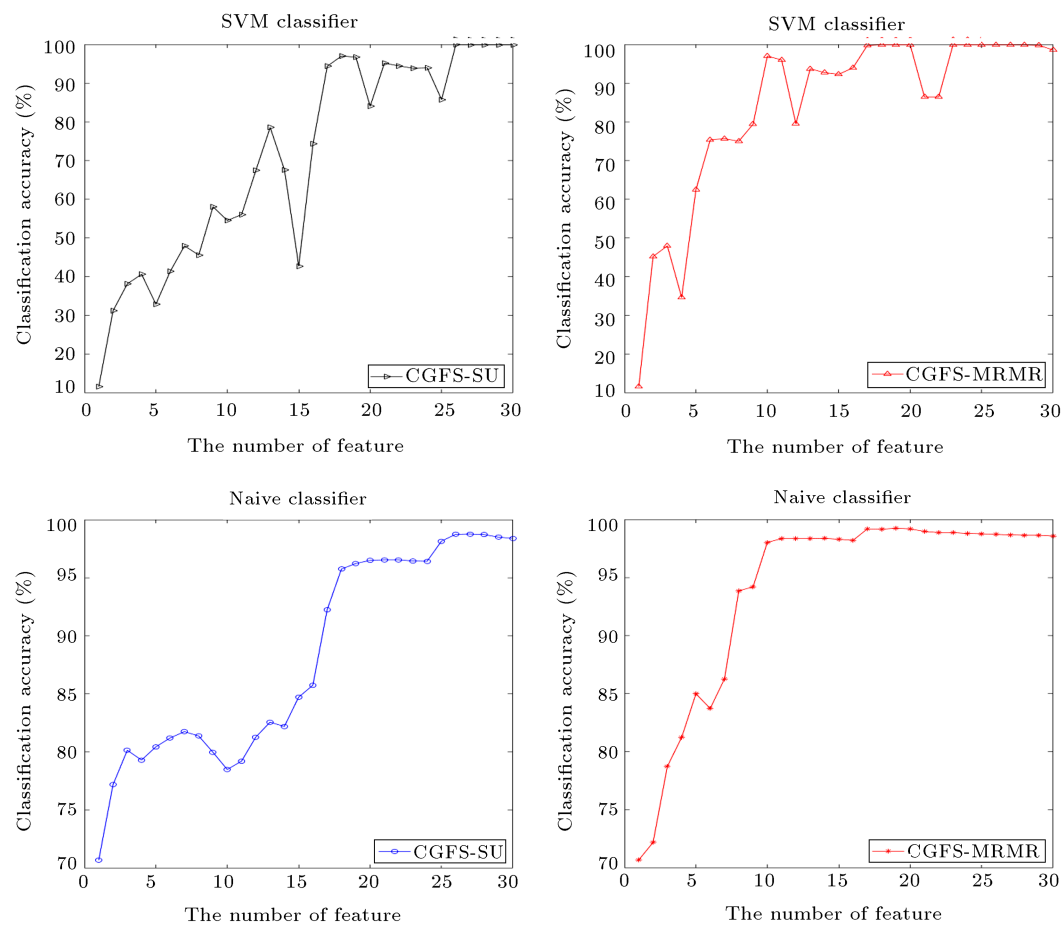
Figure 11. Classifications performance versus the numbers of selected features by the SVM and the Naïve Bayes.

Table 5. Extracted features from the EMD.

Number	EMD	Number	EMD
1	Mean value of IMF 1	21–23	Second to forth moments of IMF 3
2	Standard deviation of IMF 1	24	Area under the IMF 3 plot
3	Skewness of IMF 1	25	Mean value of IMF 4
4	Kurtosis of IMF 1	26	Standard deviation of IMF 4
5–7	Second to forth moments of IMF 1	27	Skewness of IMF 4
8	Area under the IMF 1 plot	28	Kurtosis of IMF 4
9	Mean value of IMF 2	29–31	Second to forth moments of IMF 4
10	Standard deviation of IMF 2	32	Area under the IMF 4 plot
11	Skewness of IMF 2	33	Mean value of IMF 5
12	Kurtosis of IMF 2	34	Standard deviation of IMF 5
13–15	Second to forth moments of IMF 2	35	Skewness of IMF 5
16	Area under the IMF 2 plot	36	Kurtosis of IMF 5
17	Mean value of IMF 3	37–39	Second to forth moments of IMF 5
18	Standard deviation of IMF 3	40	Area under the IMF 5 plot
19	Skewness of IMF 3		
20	Kurtosis of IMF 3		

select features. Below is a brief presentation of the MRMR and SU feature selection methods.

5.3. MRMR

The mutual information of two variables x and y is defined in terms of their probability density functions $p(x)$, $p(y)$, and $p(x,y)$:

$$I(x; y) = \sum_{x \in X} \sum_{y \in Y} p(x, y) \log \frac{p(x, y)}{p(x)p(y)}. \quad (17)$$

Let U denote the input data tabled as M samples and K features $X = \{x_i, i = 1, ..., K\}$ and the target classification variable is denoted by h, and also S is the subset of features that we are seeking. The maximum relevance criterion aims to identify features with the highest mutual information $I(x_i, h)$ with the target class h. The maximum relevance condition is:

$$\max \ W(S, h), \quad W = \frac{1}{|S|} \sum_{x_i \in S} I(x_i, h). \quad (18)$$

However, the purpose of minimum redundancy is to select the features that have the least correlation between them. Thus, the minimum redundancy condition is:

$$\min \ V(S), \quad V = \frac{1}{|S|^2} \sum_{x_i, x_j \in S} I(x_i, x_j). \quad (19)$$

For obtaining the MRMR feature set, the operator $\mu(W, V)$ is defined to combine the two criteria mentioned above and optimize them simultaneously [48]:

$$\max \ \mu(W, V), \quad \mu = W - V. \quad (20)$$

5.4. SU

The SU is a correlation measure between features and the target concept, and it is a reliable measure for selecting relevant features. In addition, the SU can be applied as a means to evaluate the suitability of features for classification, as it is an extension of mutual information that is normalized to the entropies of feature values and/or the target class. It is defined as follows [49]:

$$SU(X, Y) = 2 \left[\frac{IG(X \,|\, Y)}{H(X) + H(Y)} \right], \quad (21)$$

where:

1. $H(X)$ is the entropy of variable X that is defined as:

$$H(X) = -\sum_i p(x_i) log_2 (p(x_i)). \quad (22)$$

2. $IG(X|Y)$ is the information gain of the feature X after observing the class Y. The information gain is defined by:

$$IG(X \,|\, Y) = H(X) - H(X \,|\, Y), \quad (23)$$

where $H(X|Y)$ is the joint probabilities of all combinations of values of X and Y.

6. Classification step

During the classification step, flicker faults are categorized using two popular algorithms, Naïve Bayes and SVM. These classifiers are considered highly effective and have been extensively utilized for various classification tasks [50]. SVM classifiers offer several benefits, including their ability to handle high-dimensional data effectively, the flexibility to use different kernel functions, and their effectiveness in handling overlapping problems [51]. Besides, the SVM parameters can be optimized through optimization techniques such as genetic algorithm. Additionally, the Naïve Bayes classifier is known for its simplicity, ease of implementation, and computational efficiency and accuracy [52]. For the Naïve Bayes classifier, the "Distribution" function is set to be "multivariate multinomial distribution". Also, the RBF kernel function is used for the SVM classifier, and the "Kernel Scale" function is set to be "auto" in the MATLAB software. The performance of the classification algorithms is estimated by 10-fold cross-validation. In this technique, the entire dataset is randomly partitioned into ten subsets of approximately equal size, in which nine subsets are used for the training data and the remaining one for the test. This process is repeated ten times and the results are averaged as the final accuracy. The definition of the Naïve Bayes was presented in [53]. Furthermore, readers interested in a detailed description of the SVM classifier can refer to the referenced study [54].

7. Simulations and results

In this research, the combinations of the flicker faults are simulated and categorized into 25 main types of faults. As mentioned in the previous sections, in order to model faults, various parameters need to be adjusted. These parameters may include the amount of fuel in the case of governor mechanical faults, the number of misfired cylinders, severity of misfiring, frequencies of pitch angle fluctuations, the number of cracked teeth, and the value of k_1 in the EAF. Furthermore, the wind speed range is considered between 6 and 15 m/s. The details of the modeled faults are presented in Table 6. A sampling frequency of 10 kHz was utilized in the study, with an Intel Core i7 2.20–GHz processor and 8–GB RAM being employed for processing the data. In the feature extraction stage, 40 features are extracted using the EMD. Next, in order to obtain the most suitable feature subset, the Cooperative Game Theory-MRMR (CGT-MRMR) and the Cooperative Game Theory-SU (CGT-SU) feature selections are used. Then, it is assumed that the feature subsets are generated by picking up just the top 30 features. The selected features from the CGT-MRMR and the CGT-SU are ordered in descending

Table 6. Simulated faults details.

No	Class	Fault type	Fault conditions	Samples for each class
1	C1	Wind shear & Tower shadow	–	200
2	C2	Blade crash	$R_3 = 1 - 6$ m	500
3	C3	Gearbox tooth crash	(1-5) tooth	500
4	C4	Fixed pitch angle	(0-5-10-15-20)	500
5	C5	Pitch angle fluctuations	(2-4-6-8-10) rad/s	500
6	C6	Misfiring	Misfiring severity: [0-100] %	
			Misfired cylinders: (1,1-4,1-4-7,1-4-7-10)	500
7	C7	Exciter mechanical fault	exciter voltage variation: ([0.9-1]pu)	500
8	C8	Governor mechanical fault	Fuel variation: ([0-1]pu)	500
9	C9	Misfiring & Exciter mechanical fault	([0-100] % - (1, 1-4, 1-4-7, 1-4-7-10)),([0.9-1]pu)	500
10	C10	Misfiring & Governor mechanical fault	([0-100] % - (1, 1-4, 1-4-7, 1-4-7-10)),([0-1]pu)	500
11	C11	EAF	$K_1 = 2900 - 3000$	500
12	C12	EAF & Misfiring	$K_1 = 2900 - 3000$, ([0-100] % - (1, 1-4, 1-4-7, 1-4-7-10))	500
13	C13	EAF & Exciter mechanical fault	$K_1 = 2900 - 3000$, ([0.9-1]pu)	500
14	C14	EAF & Governor mechanical fault	$K_1 = 2900 - 3000$, ([0-1]pu)	500
15	C15	EAF & Blade crash	$K_1 = 2900 - 3000$, $R_3 = 1 - 6$ m	500
16	C16	EAF & Gearbox tooth crash	$K_1 = 2900 - 3000$, (1-5) tooth	500
17	C17	EAF & Fixed pitch angle	$K_1 = 2900 - 3000$, (0-5-10-15-20)	500
18	C18	EAF & Pitch angle fluctuations	$K_1 = 2900 - 3000$, (2-4-6-8-10) rad/s	500
19	C19	Misfiring & Blade crash	([0-100] % - (1, 1-4, 1-4-7, 1-4-7-10)), $R_3 = 1 - 6$ m	500
20	C20	Misfiring & Fixed pitch angle	([0-100] % - (1, 1-4, 1-4-7, 1-4-7-10)), (0-5-10-15-20)	500
21	C21	Misfiring & Pitch angle fluctuations	([0-100] % - (1, 1-4, 1-4-7, 1-4-7-10)), (2-4-6-8-10) rad/s	500
22	C22	Exciter mechanical fault & Blade crash	([0.9-1]pu) , $R_3 = 1 - 6$ m	500
23	C23	Exciter mechanical fault & pitch angle fluctuations	([0.9-1]pu) , (2-4-6-8-10) rad/s	500
24	C24	Governor mechanical fault & Fixed pitch angle	([0-1]pu) , (0-5-10-15-20)	500
25	C25	Governor mechanical fault & Gearbox tooth crash	([0-1]pu) , (1-5) tooth	500

order of importance. Then, these selected features can be used by the Naïve Bayes and the SVM to classify the flicker faults. Afterward, the classification performances versus the number of features are shown in Figure 11. The figures presented have a vertical axis representing the performance of the classifiers using the first X features, while the horizontal axis displays the first X features themselves. According to Figure 11, the highest accuracy can be 99.90 with 18 features by the CGT-MRMR and 99.92% with 26 features by the CGT-SU. Selecting too many features can be worthless and decrease accuracy. Therefore, to ensure optimal performance, the size of the feature subset is important. As shown in Figure 11, when the most significant features were added to the input of the classifier one by one, the accuracies of both Naïve Bayes and SVM improved until they reached their highest performance. After that point, further feature additions either caused a decrease in accuracy or had no significant effect on accuracy. It should be noted that the purpose of feature selection is to choose the most informative subset of features for classification while removing irrelevant or redundant features. As shown in Table 5, 40 features were extracted for each IMF, resulting in an input vector dimension of 40×6100. The number 40 represents the number of selected features, while
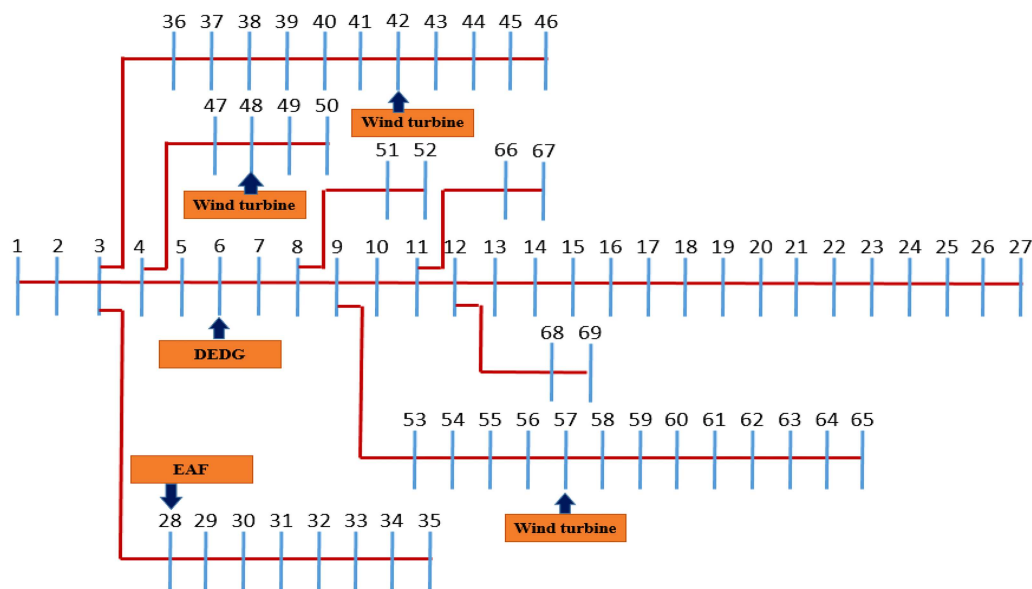
6100 indicates the number of samples. However, the dimension of features is reduced significantly through feature selection. The smallest feature vector contains only 18 features, which is 22 fewer features than the largest feature vector with 40 features. Therefore, the memory space is reduced and the speed of the process increases. Besides, to illustrate the effectiveness and feasibility of the proposed method, the performances of the two classifiers with the number of selected features are shown in Table 7. As can be seen from Table 7, the CGT-SU-SVM and the CGT-MRMR-SVM discriminate flicker faults with 99.92% and 99.90% using only the top 26 and 18 features, respectively. Also, the SVM classifier performs better than the Naïve Bayes classifier. However, the accuracies of the SVM are not significantly higher than the Naïve Bayes. According to Table 7, the selected features with the CGT-MRMR are fewer than the CGT-SU. Furthermore, the GCT-MRMR achieves higher accuracy in the Naïve Bayes classifier.

7.1. Investigating the proposed method for the IEEE-69 bus test system

The performance of the proposed approach has been evaluated on the IEEE-69 bus test system. The system information can be found in [55]. The location of flicker

Table 7. Results of classifiers.

Classifier	SVM		Naïve Bayes	
Feature selection method	CGT-SU	CGT-MRMR	CGT-SU	CGT-MRMR
Accuracy	99.92	99.90	98.76	99.23
Feature dimension	26	18	27	19
Feature vectors	CGT-SU: [19, 35 ,27, 38, 36, 28, 33, 34, 26, 37, 40, 20, 18, 25, 39, 3, 1, 2, 4, 5, 6, 7, 8, 12, 10, 16] CGT-MRMR: [3, 4, 10, 11, 12, 6, 5, 15, 16, 18, 20, 25, 26, 28, 1, 7, 8, 14]	CGT-SU: [19, 35 ,27, 38, 36, 28, 33, 34, 26, 37, 40, 20, 18, 25, 39, 3, 1, 2, 4, 5, 6, 7, 8, 12, 10, 16, 21] CGT-MRMR: [3, 4, 10, 11, 12, 6, 5, 15, 16, 18, 20, 25, 26, 28, 1, 7, 8, 14, 38]		

Figure 12. IEEE-69 bus test system.

sources is presented in Figure 12. As can be seen from this figure, different wind turbines with different faults are connected to the buses. Also, in this figure, source 1 refers to a 1.5 MW wind turbine that has a mechanical blade crash fault and is connected to bus 42 through an 11–km line. Source 2 refers to a 1.2 MW wind turbine that has a fixed pitch angle fault and is connected to bus 48 through a 14–km line. Source 3 refers to a 1.8 MW wind turbine that experiences pitch angle fluctuations and is connected to bus 57 via a 15–km line. Source 4 refers to an EAF that is connected to bus 28 through an 11–km line, and source 5 refers to a DEDG that has a misfiring fault and is connected to bus 6 via a 12–km line. Besides, for testing the effectiveness of the proposed method, the presence of the noise is considered. The Signal-to-Noise Ratio (SNR) changes from 30 dB to 50 dB.

The identification results are presented in Tables 8 and 9. The sampling frequency is 10 kHz and voltage signals are recorded at the PCC. A total of 8 classes are considered and for each one, 200 instances have been recorded. Half of them are utilized for the testing phase, and the other half is used for the testing phase. The obtained results show that our proposed method can achieve acceptable results, even in the presence of noise. The best accuracy is 99.88%, with eight features in 0.01275 s. Also, the results show the efficiency of the proposed method, which can be used in different test systems.

8. Comparison with other publications

To demonstrate the effectiveness of the proposed method, the performance of our method is compared

Table 8. Classification results.

Type of fault	Classification accuracy (%)-SVM-CGT-MRMR			
	Without noise	30 dB	40 dB	50 dB
Wind turbine with blade crash	100	100	100	100
Wind turbine with fixed pitch angle	100	100	100	100
Wind turbine with Pitch angle fluctuations	99.00	100	100	100
DEDG with misfiring	100	100	100	100
EAF	100	100	99.00	99.00
Wind turbine with pitch angle fluctuations & EAF	100	100	100	100
DEDG with misfiring & EAF	100	99.00	100	100
DEDG with misfiring & Wind turbine with mechanical blade crash	100	99.00	100	100
Number of features	7	9	8	8
Overall accuracy (%)	99.88	99.75	99.88	99.88
Time (s)	**0.01275**	**0.01475**	**0.01292**	**0.01331**

Table 9. Classification results.

Type of fault	Classification accuracy (%)-Naïve Bayes-CGT-MRMR			
	Without noise	30 dB	40 dB	50 dB
Wind turbine with blade crash	100	100	100	100
Wind turbine with fixed pitch angle	100	100	100	100
Wind turbine with Pitch angle fluctuations	99.00	100	100	100
DEDG with misfiring	100	100	98.00	100
EAF	100	100	99.00	99.00
Wind turbine with pitch angle fluctuations & EAF	100	99.00	100	100
DEDG with misfiring & EAF	99.00	97.00	100	100
DEDG with misfiring & Wind turbine with mechanical blade crash	100	100	100	98.00
Number of features	9	11	10	9
Overall accuracy (%)	99.75	99.50	99.63	99.63
Time (s)	**0.01631**	**0.01833**	**0.01667**	**0.01642**

with its counterparts in other publications, as shown in Table 10. In this table, the type of method, disadvantages, and voltage and current information are compared. In [7–10,14], both the voltage and current information were needed for their procedure; as a result, they needed more memory space and more time to process their proposed algorithm. In [6,11,15], more than one measurement point is required to get sufficient information; thus, their methods are time-consuming. In [16], only a single flicker source can be detected. Besides, using two different signal processing techniques caused their approach to be more complex. In [17], not only do authors use two signal processing techniques but also their feature selection method is considered as a wrapper method, which is

very time-consuming and suffers high computational complexity. Likewise, in [6–11,14,15], faults of the wind turbine and the DEDG causing flicker problems were not investigated. Moreover, in these papers, the detection time was not mentioned, which is an important factor because if the detection time is high, then the proposed method cannot be applicable. However, in our proposed method, only one measurement point is used, leading to less processing burden and time. Using EMD to extract informative features instead of multiple signal processing techniques can simplify the procedure and result in more valuable features being extracted. Besides, Using an efficient feature selection method to select the smallest possible feature set can reduce memory usage and processing time.

Table 10. Comparison with the other papers.

References	Methods	Measurement	Disadvantages	Detection time (s)
Samet et al. [6]	ARMA-Hilbert transform-PSD-ANN	Voltage	More than one measurement point- high computational complexity- Time consuming	–
Moghadam Banaem et al. [7]	WT-Flicker power-Approximate equivalent circuit of the line	Voltage & current	More than one measurement point- high computational complexity- demerits of WT-Time consuming	–
Moghadam Banaem et al. [8]	Discrete version of the CWT-Flicker power- Approximate equivalent circuit of the line-Computing low-frequency computations	Voltage & current	More than one measurement point- high computational complexity- demerits of CWT-Time consuming	–
Givi and Hoseini [9]	FFT-Computing the bus complex power-Diagram of complex power angle versus frequency	Voltage & current	More than one measurement point- high computational complexity- demerits of FFT-Time consuming -	–
Moghadam Banayem et al. [10]	Discrete version of the WT-Flicker power	Voltage & current	More than one measurement point- high computational complexity	–
Eghtedarpour et al. [11]	Multi-resolution S-transform-Multi Level Perceptron (MLP) neural network	Voltage	More than one measurement point- Single flicker source detection	–
Axelberg et al. [14]	Flicker power analysis	Voltage & current	Single flicker source detection	–
Kuwalek et al. [15]	Non-parametric statistical analysis-Kernel density estimation	Voltage	More than one measurement point- high computational complexity	–
Fooladi and Foroud [16]	WT-ST-Releiff method-PNN	Voltage	Demerits of WT & ST - Single flicker source detection	–
Fooladi et al. [17]	DWT-DST- Gram Schmidt method-KNN	Voltage	High computational complexity- Time consuming- Demerits of Wrapper method	–
Our proposed method	**EMD-CGT-MRMR-SVM**	Voltage	–	$0.02 \text{ s} \leq$

It should be noted that for implementing the proposed method in practice, power quality analyzers and meters products can be used, such as "FLUKE Three-Phase Power Quality Recorder," which has the ability to record voltage signals at the real networks in the power system. Also, this device is compliant with IEC 61000-4-30. This device can crosslink Ethernet cable and USB cable for direct computer connection. After that, the recorded voltage at the PCC are transferred to the computer. Then, the recorded data are analyzed by the proposed algorithm. Thus, flicker sources can be identified. Future research goals could involve exploring faster, more reliable, and simpler signal processing techniques to reduce the feature dimension and improve detection speed. However, it remains to be seen what the future holds in terms of advancements in the field.

9. Conclusion

This paper introduced a method based on the Empirical Mode Decomposition (EMD) for identifying and classifying flicker sources, especially fixed-speed wind turbines. Many factors that caused flicker in the wind turbine (such as error of the pitch angle, wind shear and tower shadow, and gearbox fault), Diesel-Engine Driven Generator (DEDG) (such as misfiring, governor, and exciter error), and the Electrical Arc Furnace (EAF) were modeled and simulated in this article. The proposed technique used only voltage waveforms; thus,

less memory space and shorter computation time for the classification were required. Overall, the results indicate that the proposed method can achieve high classification performance.

Nomenclature

$u(t)$	Main signal for EMD
$e_{low}(t)$	Local minimum of the main signal in EMD
$e_{up}(t)$	Local maximum of the main signal in EMD
$h(t)$	Mean value of envelopes for signal in EMD
$d(t)$	The detail in EMD transform
v_{eq}	Equivalent wind speed
N	Number of gearbox teeth
ω	Shaft speed
H	Elevation
H_{ref}	Elevation reference
v	Wind speed at elevation H
v_{ref}	Wind speed at an elevation H_{ref}
a	Friction factor
n	Generator rated power
T	Time
θ	Rotor position or blade azimuthal angle
V_h	Average wind speed at hub height
R	Wind turbine blade radius
β	Pitch angle
γ	Tip speed ratio
x	Blade origin from tower midline
C_p	Wind turbine rotor efficiency
s	Rotor blades area
ρ	Air density
ω	Speed of the shaft
T	Transferred torque by gearbox
M	Number of gears

References

1. Hou, S., Chu, Y., and Fei, J. "Adaptive type-2 fuzzy neural network inherited terminal sliding mode control for power quality improvement", *IEEE Trans. Ind. Informatics*, **17**(11), pp. 7564–7574 (2021).

2. Narimani, M. and Hosseinian, H. "Investigation of harmonic effects in locational marginal pricing and developing a framework for LMP calculation", *Sci. Iran.*, **29**(3), pp. 1537–1546 (2022).

3. Xu, J. and Liu, Y. "Voltage flicker mitigation strategy based on individual pitch control of wind turbine",
2021 13th Int. Conf. Meas. Technol. Mechatronics Autom., IEEE, pp. 459–462 (2021).

4. Denisov, E., Evdokimov, Y.K., Nigmatullin, R.R., et al. "Spectral method for PEMFC operation mode monitoring based on electrical fluctuation analysis", *Sci. Iran.*, **24**(3), pp. 1437–1447 (2017).

5. Moreno, C.V., Duarte, H.A., and Garcia, J.U. "Propagation of flicker in electric power networks due to wind energy conversions systems", *IEEE Trans. Energy Convers.*, **17**(2), pp. 267–272 (2002).

6. Samet, H., Khosravi, M., Ghanbari, T., et al. "A two-level neural network approach for flicker source location", *Comput. Electr. Eng.*, **92**, 107157 (2021).

7. Moghadam Banaem, H. and Tousi, B. "A new approach for the simultaneous identification of the location and individual contribution of multiple flicker sources using the least number of monitoring points", *Int. Trans. Electr. Energy Syst.*, **31**(3), p. e12767 (2021).

8. Moghadam Banaem, H., Abbasi, M., and Tousi, B. "A new method with minimum number of monitoring points for flicker source tracing by wavelet transform", *Int. Trans. Electr. Energy Syst.*, **29**(9), p. e12057 (2019).

9. Givi, H. and Hoseini, S.R.K. "An effective signature for detection of flicker sources in transmission networks using fast fourier transform", *2020 28th Iran. Conf. Electr. Eng.*, IEEE, pp. 1–6 (2020).

10. Moghadam Banayem, H., Doroudi, A., and Poormonfared Azimi, M. "Flicker source tracing by wavelet transform", *Electr. Power Components Syst.*, **43**(4), pp. 412–421 (2015).

11. Eghtedarpour, N., Farjah, E., and Khayatian, A. "Intelligent identification of flicker source in distribution systems", *IET Gener. Transm. Distrib.*, **4**(9), pp. 1016–1027 (2010).

12. Thirumala, K., Pal, S., Jain, T., et al. "A classification method for multiple power quality disturbances using EWT based adaptive filtering and multiclass SVM", *Neurocomputing*, **334**, pp. 265–274 (2019).

13. Zhang, S., Li, P., Zhang, L., et al. "Modified S transform and ELM algorithms and their applications in power quality analysis", *Neurocomputing*, **185**, pp. 231–241 (2016).

14. Axelberg, P.G.V., Bollen, M.H.J., and Gu, I.Y.-H. "Trace of flicker sources by using the quantity of flicker power", *IEEE Trans. Power Deliv.*, **23**(1), pp. 465–471 (2007).

15. Kuwalek, P. "Trace of flicker sources by using nonparametric statistical analysis of voltage changes", *2020 19th Int. Conf. Harmon. Qual. Power*, IEEE, pp. 1–6 (2020).

16. Fooladi, M. and Foroud, A.A. "Recognition and assessment of different factors which affect flicker in wind turbines", *IET Renew. Power Gener.*, **10**(2), pp. 250–259 (2016).

17. Fooladi, M., Foroud, A.A., and Abdoos, A.A. "Detection and evaluation of effective factors on flicker phenomenon in diesel-engine driven generators", *Appl. Therm. Eng.*, **113**, pp. 1194–1207 (2017).

18. Hafiz, F., Swain, A., Naik, C., et al. "Efficient feature selection of power quality events using two dimensional (2D) particle swarms", *Appl. Soft Comput.*, **81**, 105498 (2019).

19. Leinonen, A. and Laketic, N. "Advanced technology to ensure EAF grid flicker compliance", *Proc. - 2018 IEEE Int. Conf. Environ. Electr. Eng. 2018 IEEE Ind. Commer. Power Syst. Eur. EEEIC/I CPS Eur. 2018* (2018).

20. Karimi, H., Simab, M., and Nafar, M. "Enhancement of power quality utilizing photovoltaic fed D-STATCOM based on zig-zag transformer and fuzzy controller", *Sci. Iran.*, **29**(5), pp. 2465–2479 (2022).

21. Altintas, E., Salor, Ö., Cadirci, I., et al. "A new flicker contribution tracing method based on individual reactive current components of multiple EAFs at PCC", *IEEE Trans. Ind. Appl.*, **46**(5), pp. 1746–1754 (2010).

22. Moradifar, A., Foroud, A.A., and Fouladi, M. "Identification of multiple harmonic sources in power system containing inverter-based distribution generations using empirical mode decomposition", *IET Gener. Transm. Distrib.*, **13**(8), pp. 1401–1413 (2019).

23. Sun, X., Liu, Y., Li, J., et al. "Using cooperative game theory to optimize the feature selection problem", *Neurocomputing*, **97**, pp. 86–93 (2012).

24. Tiwari, V.K. and Gupta, A.R. "Application of SVC and STATCOM for Wind Integrated Power System", *Recent Adv. Power Electron. Drives, J. Kumar and P. Jena, Eds.*, Springer Singapore, Singapore, pp. 181–192 (2021).

25. Alam, M.J.E., Muttaqi, K.M., and Sutanto, D. "Battery energy storage to mitigate rapid voltage/power fluctuations in power grids due to fast variations of solar/wind outputs", *IEEE Access*, **9**, pp. 12191–12202 (2021).

26. Sϕrensen, P., Andresen, B., Fortmann, J., et al. "Modular structure of wind turbine models in IEC 61400-27-1", *2013 IEEE Power Energy Soc. Gen. Meet.*, IEEE, pp. 1–5 (2013).

27. Mostafaeipour, A., Rezaei, M., Jahangiri, M., et al. "Feasibility analysis of a new tree-shaped wind turbine for urban application: A case study", *Energy Environ.*, **31**(7), pp. 1230–1256 (2020).

28. Lee, T. "Financial investment for the development of renewable energy capacity", *Energy Environ.*, **32**(6), pp. 1103–1116 (2021).

29. Jang, H. "Firm structure, scale economies, and productivity in the US electric power industry: A cost function analysis", *Energy Environ.*, **32**(5), pp. 834–854 (2021).

30. Charles Rajesh Kumar, J., Vinod Kumar, D., Baskar, D., et al. "Offshore wind energy status, challenges, opportunities, environmental impacts, occupational health, and safety management in India", *Energy Environ.*, **32**(4), pp. 565–603 (2021).

31. Qolipour, M., Mostafaeipour, A., Saidi-Mehrabad, M., et al. "Prediction of wind speed using a new Grey-extreme learning machine hybrid algorithm: A case study", *Energy Environ.*, **30**(1), pp. 44–62 (2019).

32. Albani, A., Ibrahim, M.Z., Yong, K.H., et al. "The wind energy potential in Kudat Malaysia by considering the levelized cost of energy for combined wind turbine capacities", *Energy Environ.*, **32**(7), pp. 1149–1169 (2021).

33. Saneie, H., Daniar, A., and Nasiri-Gheidari, Z. "Design optimization of a low speed small scale modular axial flux permanent magnet synchronous generator for urban wind turbine application", *Sci. Iran.*, **29**(6), pp. 3326–3337 (2022).

34. Das, S., Karnik, N., and Santoso, S. "Time-domain modeling of tower shadow and wind shear in wind turbines", *ISRN Renew. Energy*, **2011**, pp. 1–11 (2011).

35. Dolan, D.S.L. and Lehn, P.W. "Simulation model of wind turbine 3p torque oscillations due to wind shear and tower shadow", *2006 IEEE PES Power Syst. Conf. Expo.*, IEEE, pp. 2050–2057 (2006).

36. Wen, B., Wei, S., Wei, K., et al. "Power fluctuation and power loss of wind turbines due to wind shear and tower shadow", *Front. Mech. Eng.*, **12**(3), pp. 321–332 (2017).

37. Rao, S.S., *Mechanical Vibrations*, Addison-Wesley World Student Series, Addison-Wesley (1995).

38. Kim, S.-K. and Kim, E.-S. "PSCAD/EMTDC-based modeling and analysis of a gearless variable speed wind turbine", *IEEE Trans. Energy Convers.*, **22**(2), pp. 421–430 (2007).

39. Sitharthan, R., Geethanjali, M., and Karpaga Senthil Pandy, T. "Adaptive protection scheme for smart microgrid with electronically coupled distributed generations", *Alexandria Eng. J.*, **55**(3), pp. 2539–2550 (2016).

40. Casado, A.J., Nieto, F.J., Blázquez, F., et al. "A monitoring system for diesel engine driven generators based on electric power output oscillation assessment", *IEEE Trans. Ind. Appl.*, **53**(3), pp. 3182–3188 (2017).

41. Sezer, İ. "A review study on using diethyl ether in diesel engines: effects on fuel properties, injection, and combustion characteristics", *Energy Environ.*, **31**(2), pp. 179–214 (2020).

42. Jhapte, R., Patel, R.N., and Neema, D.D., *Design and Analysis of Optimized Hybrid Active Power Filter for Electric Arc Furnace Load*, Springer, Singapore, pp. 250–258 (2018).

43. Hajipour, R., Asadollahzadeh Shamkhal, F., and Kobravi, H.R. "A methodology for examining the chaotic behavior of CoP signal during quiet standing based on empirical mode decomposition method", *Sci. Iran.*, **28** (Special issue on collective behavior of nonlinear dynamical networks), pp. 1560–1569 (2021).

44. Hu, Z., Ma, J., Yang, L., et al. "Monthly electricity demand forecasting using empirical mode decomposition-based state space model", *Energy Environ.*, **30**(7), pp. 1236–1254 (2019).

45. Motlagh, S.Z.T. and Foroud, A.A. "Power quality disturbances recognition using adaptive chirp mode pursuit and grasshopper optimized support vector machines", *Measurement*, **168**, 108461 (2021).

46. Moradifar, A., Foroud, A.A., and Firouzjah, K.G. "Comprehensive identification of multiple harmonic sources using fuzzy logic and adjusted probabilistic neural network", *Neural Comput. Appl.*, **31**(1), pp. 543–556 (2019).

47. Yu, J.C.P., Wee, H.M., Jeng, S., et al. "Two-stage game-theoretic approach to supplier evaluation, selection and order assignment", *Sci. Iran.*, **28**(6), pp. 3513–3524 (2021).

48. Gu, X., Guo, J., Xiao, L., et al. "Conditional mutual information-based feature selection algorithm for maximal relevance minimal redundancy", *Appl. Intell.*, pp. 1–12 (2021).

49. Zhang, L. and Chen, X. "Feature selection methods based on symmetric uncertainty coefficients and independent classification information", *IEEE Access*, **9**, pp. 13845–13856 (2021).

50. Rasaizadi, A., Sherafat, E., and Seyedabrishami, S. "Short-term prediction of traffic state, statistical approach versus machine learning approach", *Sci. Iran.*, **29**(3), pp. 1095–1106 (2022).

51. Das, S., Datta, S., Zubaidi, H.A., et al. "Applying interpretable machine learning to classify tree and utility pole related crash injury types", *IATSS Res.* (2021).

52. Putri, D.A., Kristiyanti, D.A., Indrayuni, E., et al. "Comparison of naive abyes algorithm and support vector machine using PSO feature selection for sentiment analysis on E-Wallet review", *J. Phys. Conf. Ser., IOP Publishing*, p. 12085 (2020).

53. Narayan, S. and Sathiyamoorthy, E. "A novel recommender system based on FFT with machine learning for predicting and identifying heart diseases", *Neural Comput. Appl.*, **31**(1), pp. 93–102 (2019).

54. Cervantes, J., Garcia-Lamont, F., Rodríguez-Mazahua, L., et al. "A comprehensive survey on support vector machine classification: Applications, challenges and trends", *Neurocomputing*, **408**, pp. 189–215 (2020).

55. Mithulananthan, N., Hung, D.Q., and Lee, K.Y., *Intelligent Network Integration of Distributed Renewable Generation*, Springer (2016).

Biographies

Shayan Zeraat Talab Motlagh received his BSc and MSc degrees in Electrical Engineering from Semnan University, Semnan, Iran in 2015 and 2019, respectively. His research interests include power quality, power systems operations, planning, and renewable energy integration.

Asghar Akbari Foroud was born in Hamadan, Iran in 1972. He received a BSc degree from Tehran University as well as MSc and PhD degrees from Tarbiat-Modares University, Tehran, Iran. He is now working at Semnan University (Professor). His research interests include power system dynamics and operation and power quality.